Applied Geography 101 (2018) 36–44

Contents lists available at ScienceDirect

Applied Geography

journal homepage: www.elsevier.com/locate/apgeog

A global erodibility index to represent sediment production potential of different rock types

Nils Moosdorf[a,*], Sagy Cohen[b], Christoph von Hagke[c]

[a] Leibniz Center for Tropical Marine Research (ZMT), Department of Biogeochemistry / Geology, Bremen, Germany
[b] University of Alabama, Department of Geography, Tuscaloosa, USA
[c] RWTH Aachen, Institute of Structural Geology, Tectonics and Geomechanics, Aachen, Germany

ARTICLE INFO

Keywords:
Erosion
Lithology
Global scale
Sediment flux
Earth surface modeling

ABSTRACT

Erosion drives landscape evolution and is fundamental for understanding the interplay between climate and tectonics as well as land-ocean matter fluxes. Large scale erosion models are an important part of the suite of Earth system models. However, their representation of the sediment production potential of different rock types is very limited. A new global erodibility index is proposed herein. It depicts the relative erosion potential of different lithological classes in the Global Lithological Map (GLiM). The erodibility index was developed by correlating observational hillslope data against climatic and tectonic setting. Hillslope data were compared for different lithological classes in regions of similar uplift across a range of landscapes. An erodibility index was defined for each lithological class, based on the relative hillslope compared to that of acid plutonic rocks in the respective area, which are here used as base lithology. The erodibility indices of different lithological classes fall within three groups: low erodibility - 1.0 for acid plutonic rocks, metamorphic rocks, and carbonate sedimentary rocks, 1.1 for acid volcanic rocks, 1.2 for mixed sedimentary rocks; medium erodibility - 1.5 for basic plutonic rocks and siliciclastic rocks of all grain sizes, 1.4 for basic volcanic rocks; high erodibility – 3.2 for unconsolidated sediments. This erodibility index is the first estimate of sediment production potential of different rock types aimed at regional to global scale application. The erodibility index presented here can help improve our understanding of global erosion and landscape evolution. A new lithology erodibility layer, the global erodibility index dataset (GEroID), is produced and used as input in a global sediment flux model (WBMsed) to demonstrate a potential utilization of the new dataset. Using an updated lithological map paired with the new erodibility index yields improved regional model results compared to the original model input.

1. Introduction

Erosion is a key process in landscape dynamics and exerts major control on sediment transport within continents and to the oceans. Erodibility is defined here as the lithology-based susceptibility of a landscape to erosion for a given set of environmental conditions. Quantifying rock erodibility is crucial to the performance of large scale geomorphology modeling and our quantitative understanding of global sediment transport.

Erosion rates have been shown to be closely connected to slope stability in mountainous terrain (Carretier et al., 2013). Many controls of rock erosion have been quantified in laboratory or field studies as well as using numerical models (e.g. de Vente & Poesen, 2005; Whipple & Tucker, 2002; Yanites et al., 2011). Local studies show that variations in rainfall can alter erosion rates on short and long timescales (Deal, Favre, & Braun, 2017; DiBiase, Whipple, Heimsath, & Ouimet, 2010; Tucker & Bras, 2000). Furthermore, availability of bedload can control erosion rates in un-fractured rocks, where moving sediment grains have been recognized as a main influence factor of bedrock erosion (e.g. Cook, Turowski, & Hovius, 2013; Sklar & Dietrich, 2001; Turowski, Hovius, Meng-Long, Lague, & Men-Chiang, 2008), whereas in fractured rocks, plucking is more dominant (e.g. Hartshorn, Hovius, Dade, & Slingerland, 2002). Few regional studies exist specifically addressing the influence of rock type on erosion rates, i.e. erodibility. In the eastern alps, Korup and Schlunegger (2009) highlighted the different erodibility of sediments and crystalline rocks. A study from the Swiss Central Alps uses a simplified geotechnical map to define four erodibility classes, and shows these correlate with topographic parameters (Kühni & Pfiffner, 2001). However, local measurements of sediment flux or erosion rate are difficult to extrapolate from catchments to entire

* Corresponding author.
E-mail address: nils_sci@moosdorf.de (N. Moosdorf).

https://doi.org/10.1016/j.apgeog.2018.10.010
Received 1 July 2017; Received in revised form 26 October 2018; Accepted 30 October 2018

orogens, and findings from locally focused studies are not necessarily transferable to analysis or modeling of orogen-continental or global scale sediment fluxes.

Extrapolation to global sediment models requires statistically robust correlations to spatial attributes representing the suggested factors. At these large scales, river sediment flux has been used to estimate present day basin-wide erosion (e.g. Gaillardet, Dupre, Allegre, & Negrel, 1997). The main controls on sediment flux in rivers are basin size and elevation range (Milliman & Syvitski, 1992), as well as land-cover (Cerdan et al., 2010; Douglas, 1967; Milliman, Qin, Ren, & Saito, 1987; Saunders & Young, 1983), among other factors (cf. de Vente et al., 2013). However, the value of river sediment load as erosion indicator is impeded by intra-basin sediment storage and re-deposition of sediment within the basin (e.g. Sadler, 1981; Schumer & Jerolmack, 2009; Wright & Marriott, 1993). At millennial to million year timescales, thermochronometry as well as dating using cosmogenic radionuclides have been applied to estimate erosion rates (e.g. Acosta et al., 2015; Reiners & Brandon, 2006; Schaller, von Blanckenburg, Hovius, & Kubik, 2001; von Blanckenburg, 2005). Compilations of global erosion rate estimates suggest rock type, tectonic setting and climate may influence erosion rates over decadal to million year timescales (Herman et al., 2013; Portenga & Bierman, 2011). The climatic influence, however, is not linear but also the variability of climate can increase erosion rates, in particular in glaciated landscapes (Ganti et al., 2016), and tectonic setting could also impact physical erosion through its coupling with chemical weathering (Raymo, Ruddiman, & Froelich, 1988; West, Galy, & Bickle, 2005). This may be viewed as an analogue to a bias of erosion rates due to intra-basin storage but for the erosional branch of a catchment-basin system. This implies direct comparison of erosion rates measured over different timescales is not possible, and additional corrections of this bias need to be found. Moreover, even though processes occurring at large temporal scales often cover large spatial scales, rock types exposed at surface vary over million year timescales, which might bias long-term erosion rate estimates. Rock uplift rates depend on plate tectonic forcing and associated crustal thickening, but also on isostatic compensation, independent of a thickening crust. Much of the present day topography, particular in areas where plate convergence is not dominant, can be explained by flow in the Earth's mantle (Hager, Clayton, Richards, Comer, & Dziewonski, 1984), see Braun (2010) for a review. Erosion influences rock uplift, as it reduces crustal thickness, which will be isostatically compensated (England & Molnar, 1990). As climate is linked to erosion, rock uplift can be seen as a function of climate and tectonics (e.g. Whipple & Meade, 2006).

Rocks such as granite or basalt often stand out in the landscape. This is a result of their low erodibility, even though to some degree it may be a result of local isostatic uplift as compensation of their erosion (Braun, Simon-Labric, Murray, & Reiners, 2014). However, at continental to global scale quantitative difference of erodibility between different rock types and consequently their different sediment production rate for the same given environmental conditions is only poorly constrained. This knowledge is important for our understanding of Earth's topography and its evolution, as well as global sediment flux estimates. Local scale and short term (i.e. decadal timescale) modeling of sediment flux and soil erosion can explicitly calibrate soil parameters affecting sediment production and transport (e.g. soil erodibility indices in the RUSLE and WEPP models: Flanagan & Nearing, 1995; Renard, Foster, Weesies, & Porter, 1991). Global scale and long term (i.e. millennial to million-year timescale) sediment flux models on the other hand cannot calibrate such parameters due to spatial and/or temporal heterogeneity. These models therefore have to rely on averaged or highly simplified (i.e. categorical) parameterization of soil or lithological classes. For example the BQART global-scale sediment flux model (Syvitski & Milliman, 2007) includes a 'Lithology Factor (L)' which, based on general understanding of the relationship between rock characteristics and sediment production, describes the contribution of basin-lumped lithological classes (from the lithological map of Dürr, Meybeck, & Dürr, 2005) to sediment flux at the basin outlet using discrete categories [0.5, 0.75, 1.0, 1.5, 2.0, 3.0] for an entire river basin. While this approach works well for the basin-lumped and semi-empirical BQART model, it cannot be readily translated to more spatially explicit and/or physically based models. For example, Cohen, Willgoose, and Hancock (2013) reported that spatially explicit implementation of the Syvitski and Milliman (2007) lithology factor within the WBMsed global riverine model yielded a low correlation ($R^2 = 0.22$) against the original Syvitski and Milliman (2007) values, even though they use the same input lithological map. Other modeling approaches define general erosion efficiency factors or detachment rate (Tucker, Lancaster, Gasparini, & Bras, 2001; Whipple & Tucker, 2002) without regarding rock type as controlling factor. Recently, quantification of a global erodibility coefficient based on erosion rate estimates from ^{10}Be data has been proposed, particularly highlighting differences of erodibility between granitic and sedimentary rocks (Harel, Mudd, & Attal, 2016).

In order to improve the spatial representation of lithology in continental to global-scale geomorphic modeling, an estimate of erodibility is needed that distinguishes different lithological classes. Multiple case studies document the fundamental necessity of constraining erosion on decadal (Dadson et al., 2003), millennial (Champagnac et al., 2009; Wittmann, von Blanckenburg, Kruesmann, Norton, & Kubik, 2007), or million year (Herman et al., 2013; von Hagke, Oncken, Ortner, Cederbom, & Aichholzer, 2014) timescales. The correlation between slope and erosion has been recognized for more than a century (e.g. Geological and Geographical Survey of the Territories (U.S.), 1876; Montgomery & Brandon, 2002), basic concepts are well established (Molnar & England, 1990; Montgomery & Brandon, 2002; Whipple, 2009; Willett & Brandon, 2002). The dynamic equilibrium between rock uplift and erosion has already been used at regional scale to predict erodibility (Lague, Davy, & Crave, 2000). Here, we apply this concept at global scale and present a lithology based erodibility index relative to that of acid plutonic rocks (mostly granite), which was calibrated on regional slope values, and its application in a global erosion model.

2. Methods

Following the assumption that steeper slopes of rocks for a given environmental setting imply less erodibility, a new erodibility index was calibrated based on slope data in different regions of homogeneous rock uplift within five landscapes between which tectonic activity, climate, and land cover vary. Within the regions, we assume that these factors vary only little at the scale of observation, and do not systematically impact slope steepness between the different lithological units. We selected landscapes where present day rock uplift rates have been determined at high resolution using geodetic measurements, providing coherent vertical velocity patterns. This data can be used to derive orogen-scale rock uplift maps that allow for inferring the underlying geodynamic driving processes causing topography, or derive patterns of fault locking (e.g. Avouac, 2008; Serpelloni, Faccenna, Spada, Dong, & Williams, 2013). The landscapes used for calibration and, respectively, the high-resolution rock uplift maps used to define regions of homogeneous rock uplift are the Central Alps (Schlatter, Schneider, Geiger, & Kahle, 2005), Himalaya (Stevens & Avouac, 2015), Mediterranean (Serpelloni et al., 2013), Sierra Nevada (Hammond, Blewitt, Li, Plag, & Kreemer, 2012), and Taiwan (Ching et al., 2011) (Table 1, Fig. 1). Within each landscape we defined an absolute measure for high, medium and low rock uplift rates. These values differ between the landscapes: whereas in the Alps rock uplift ranges from < 1 mm/yr (low rock uplift) to > 2 mm/yr (high rock uplift), in Taiwan are an order of magnitude higher and ranges from < 10 mm/yr (low rock uplift) to > 15 mm/yr (high rock uplift) (Table 1). Rock uplift rates are extremely high in Taiwan due extremely high convergence rates, whereas in the Central Alps convergence is slow and consequently rock uplift rates are much lower. Climatic regime is an additional factor

Table 1
Erodibility index for the different calibration regions and the world. Only the global average will be used further.

Region	Uplift class	Uplift range (mm/a)	Avg. Slope (°)	Erodibility index (unitless)										
				mt	pa+	pb	sc	sm	ss	sssh	ssss	su	va	vb+
Alps	low	< 1	20.6	0.8	1[a]	0.8	1.0	1.5	0.9		0.9	3.0	1.2	2.2
	med	1–2	26.0	1.1	1[a]	1.1	1.4	1.7	1.3		2.4	2.0	1.0	1.2
	high	> 2	28.5	1.1	1[a]	1.1	1.2	1.1	1.4		1.4	1.9	1.4	1.1
Himalaya	low	< 1	25.8	1.1	1[a]	1.1	1.0	1.0	1.6	1.2	1.2	5.1	1.0	1.1
	med	1–2	26.8	1.0	1[a]	0.9	1.1	1.1	1.7	1.3	1.1	3.4		1.1
	high	> 2	27.1	0.9	1[a]	1.9	1.1	1.2	1.3	1.4	1.5	2.1		1.1
Mediterranean	low	< 1	11.3	0.9	1[a]	0.6	0.9	1.4	1.4		0.8	2.7		
	med	1–2	13.6	1.0	1[a]		1.0	1.0	1.8	0.9	0.7	1.9	1.4	1.8
	high	> 2	9.0											
Sierra Nevada	low	< 0.5	10.8	0.8	1[a]	1.0	0.8	1.2	1.0	1.0	1.5	3.3	1.1	1.3
	med	0.5–1.5	12.7	1.1	1[a]	1.2	0.9	1.3	1.2	1.1	2.0	3.4	1.1	1.3
	high	> 1.5	14.4	0.8	1[a]	1.1	0.9	1.0	1.2	1.1	2.8	4.2	0.8	1.2
Taiwan MT	low	< 10	19.1	1[a]		2.4		1.1	1.7	1.5		3.5		1.3
	med	10–15	26.9	1[a]		2.5		1.0	1.4	2.9		3.1		1.6
	high	> 15	30.5	1[a]		3.7		1.1	1.2	2.3		5.2		1.3
	Standard deviation			0.1	0	0.9	0.1	0.2	0.3	0.6	0.6	1.0	0.2	0.3
	GLOBAL AVERAGE (= EI)			**1.0**	**1.0**	**1.5**	**1.0**	**1.2**	**1.4**	**1.5**	**1.5**	**3.2**	**1.1**	**1.4**

Definitions of lithological classes [adapted from Hartmann & Moosdorf, 2012].
mt: Metamorphic rocks, mainly gneiss.
pa+: acid and intermediate plutonic rocks, mainly granite and syenite.
sc: carbonate-rich sedimentary rocks, mainly limestone and dolomite.
sm: mixed carbonate and siliciclastic sedimentary rocks, e.g. marl.
ss: siliciclastic sedimentary rocks, mixed or unknown grain sizes, e.g. shale-sandstone interbedding.
sssh: siliciclastic sedimentary rocks, fine grained, mostly siltstone or shale.
ssss: siliciclastic sedimentary rocks, coarse grained, mostly sandstone or conglomerate.
su: unconsolidated sedimentary rocks, all grain sizes.
va: acid volcanic rocks, mostly rhyolite.
vb+: basic and intermediate volcanic rocks, mostly basalt and andesite.
The classes ss, sssh and ssss were re-combined into a single class for further calculations.
[a] Lithological class used for normalization; the erodibility index is 1 per definition.

influencing rock uplift rates, possibly introducing bias if absolute values between different landscapes were compared. Consequently, to account for differences in tectonic rates, for our study, we use only relative values, i.e. areas of relatively high vs relatively low rock uplift for a certain landscape. Using ArcGIS 10.3, polygons of regions representing three rock uplift classes (low, medium, high) per landscape were digitized from rock uplift maps. Individual calibration regions were chosen to be large enough (i.e. encompassing multiple faults), so that potential bias introduced by transient rock uplift peaks associated with movement along a single fault are averaged out and can be considered negligible. For all regions, the average slope per lithological class in the global lithological map GLiM v1.0 (Hartmann & Moosdorf, 2012) was derived, using the "Zonal Statistics as Table" tool of ArcGIS. Some of the original lithological classes were combined with similar lithologies to reduce the number of classes: Acid and intermediate plutonics, as well as basic and intermediate volcanics were combined into one class each.

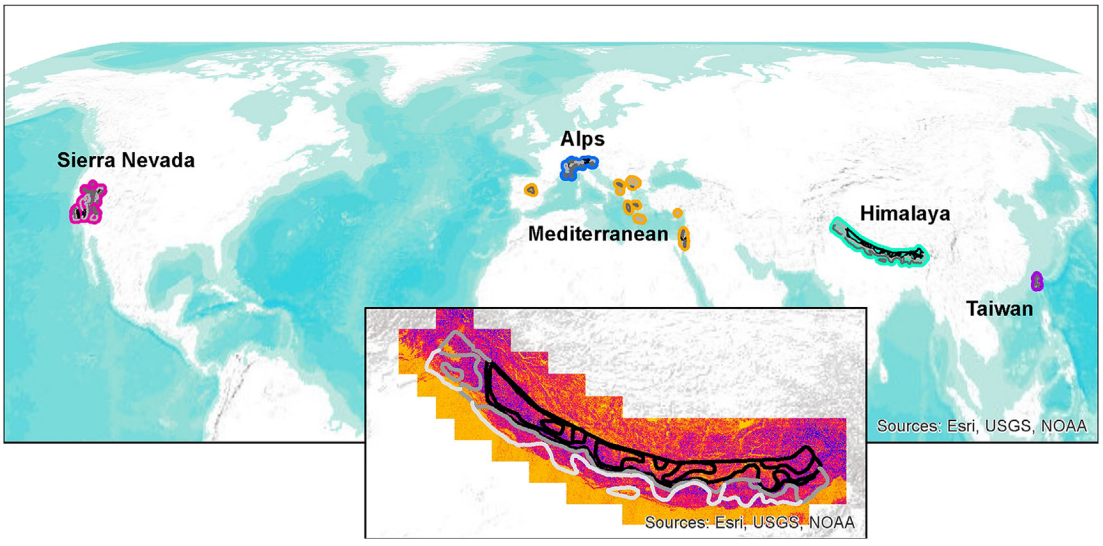

Fig. 1. Calibration landscapes of the erodibility index. The inlet shows the GDEM DEM slopes in the Himalaya landscape and a representation of the uplift regions (black: high, grey: medium, light grey: low) mapped from Stevens and Avouac (2015).

Siliciclastic sediments are represented here as three classes, based on the dominant grain size (mixed, fine or coarse grained). The definition of the lithology classes is taken from the original publication (Hartmann & Moosdorf, 2012) and provided in short in the footnotes of Table 1. Topography data were acquired from relevant tiles of the ASTER GDEM v2 with a horizontal resolution of 30 m (http://gdem.ersdac.jspacesystems.or.jp/downloaded in January 2016). They were mosaicked and projected to World Eckert IV projection. The slope between neighboring cells was calculated using the "slope" tool of the ArcGIS 3D Analyst.

For each investigated region i and rock uplift class j the erodibility index (EI) was calculated by normalizing average slope (s) per lithological class (l) with that of acid plutonics (pa):

$$EI_{l,\,i,j} = \frac{s_{pa,\,i,j}}{s_{l,\,i,\,j}} \tag{1}$$

Thus, the lower the average slope of a given lithological unit compared to that of acid plutonic rocks, the higher the erodibility index. This procedure follows the seminal paper on chemical rock weathering, which normalizes chemical weathering to acid plutonics (granite: Meybeck, 1987). Implicitly, defining a single erodibility index per lithological class depending only on average slopes in a specific tectonic and regional setting neglects other local complexities, which can contribute to rock erodibility, as referenced in the introduction. However, we assume that at large scales, many local complexities counterbalance each other.

In Taiwan, no acid plutonic rocks were mapped within the analyzed polygons in the global lithological map. There, metamorphic rocks were used as normalization instead, because in other regions, the average slope of acid plutonic rocks and metamorphic rocks is very similar. For the areas with high rock uplift rates in the Mediterranean Region (i.e. Central Spain, Dinarides, Hellenides, Cyprus and parts of the Taurides, and Israel) an erodibility index could not be calculated because neither acid plutonics nor metamorphic rocks are mapped in GLiM. Although rock uplift data is available for Fennoscandia (Fjeldskaar, Lindholm, Dehls, & Fjeldskaar, 2000) and the Apennines, Italy (Serpelloni et al., 2013), the lithological map does not provide the necessary data quality to derive slopes per lithological unit. The erodibility index presented in this study equals averages from all calibration landscapes and uplift regions per lithological class.

Uncertainty of the slope input data were addressed with a Monte Carlo approach. The vertical uncertainty of the original GDEM elevation dataset was assumed to be 10 m, following studies in the Himalaya (Mukul, Srivastava, Jade, & Mukul, 2017), in order to use a conservative value. To derive standard deviations of the slope data per calibration region an uncertainty raster of −10 to +10 was added to the DEM, and a slope raster was calculated from the product. This was used to derive an average slope per region. The process was repeated 10–30 times per landscape (depending on computational requirements), following Temme, Heuvelink, Schoorl, and Claessens (2009). The standard deviation of the calculated mean slopes per region provides a basis for a second Monte Carlo analysis that calculated the distribution of Erodibility Indices based on 10,000 draws attributing a normal distribution of slopes (s) per region using the previously derived standard deviations (σ) around the mean ($\bar{s}$, based on the slope calculated using the original dataset) of each landscape (i), uplift region (j) and lithology (l):

$$s_{i,j,l,1-10000} = \bar{s}_{i,j,l} \pm \sigma_{i,\,j,l} \tag{2}$$

The distribution of these values is propagated to the erodibility index, which is by that calculated 10,000 times for different combinations of slopes, based on Eq. (1).

To demonstrate the use of the resulting global erodibility index layer (named global erodibility index dataset: GEroID), we incorporate it as an input layer for the WBMsed model (Version 2: Cohen, Kettner, & Syvitski, 2014)). WBMsed is a spatially and temporally explicit riverine modeling framework capable of predicting global-scale riverine fluxes of water, sediment and nutrients (Cohen et al., 2013). The sediment module in WBMsed is based on the BQART equation (Syvitski & Milliman, 2007)

$$\bar{Q}_s = \omega B \bar{Q}^{0.3} A^{0.5} RT \quad \text{for } T \geq 2°\text{C}, \tag{3a}$$

$$\bar{Q}_s = 2\omega B \bar{Q}^{0.3} A^{0.5} R \quad \text{for } T < 2°\text{C}, \tag{3b}$$

where $\bar{Q}_s$ is average suspended sediment loads or a basin outlet, ω is coefficient of proportionality that equals 0.02 for units of kg s^{-1}, $\bar{Q}$ is long-term average discharge for each cell ($m^3\ s^{-1}$), A is basin upstream contributed area of each cell (km^2), R is relative relief difference between the highest relief of the contributing basin to that cell and the elevation of that particular cell (km), and T is average temperature of the upstream contributing area (°C). The B term

$$B = IL(1 - T_E)E_h \tag{4}$$

includes the lithology factor L (equals the erodibility index), I denotes glacial erosion processes, T_E is sediment trapping in reservoirs and E_h is a human-influenced soil erosion factor. See Syvitski and Milliman (2007) for details regarding the BQART parameters and Cohen et al. (2013) for their spatially explicit implementation in the WBMsed model.

Different input datasets were used over the years to represent the L factor. When first introduced, Syvitski and Milliman (2007) estimated basin-averaged L value based on Dürr et al. (2005) global lithology by assessing the dominant lithological units within each basin. They categorized the L into five value classes: 0.5, 0.75, 1.0, 1.5, 2.0 and 3.0. Cohen et al. (2013) initially used Syvitski and Milliman (2007) classification scheme to re-classify the Dürr et al. (2005) map as a spatially explicit L-value map. They have found, however, that the resulting L factor input was one of the major sources of bias in the model sediment flux prediction and therefore reverted to a basin-lumped input, similar to Syvitski and Milliman (2007). Unlike the Syvitski and Milliman (2007) categories, the global erodibility index categories range from 1 to 3.2. Using a minimum value of 1 offers a more generic index, not linked to a specific model parameter. Here we use the global erodibility index layer as an input to the WBMsed model without adjusting its values or the model coefficients as demonstration of the effect of the new Erodibility Index; adjusting other model coefficients is beyond the scope of this work. We compare averaged model predictions using the global erodibility index layer to model predictions using the original input layer. The intention of this comparison is not to evaluate differences in the model prediction accuracy (which is not feasible without recalibrating the dataset or the model equations) but to demonstrate the increased intra-basin spatial dynamics resulting from the new dataset, and present the estimates of rock erodibility that are calibrated on regions from three continents for global scale usage.

3. Results and discussion

3.1. The erodibility index

For the different lithological classes (representing rock units at regional scale) the erodibility index amounts to:

- 1.0 - acid plutonic rocks, metamorphic rocks, and carbonate sedimentary rocks;
- 1.1 - acid volcanic rocks;
- 1.2 - mixed sedimentary rocks;
- 1.4 - basic volcanic rocks;
- 1.5 - basic plutonic rocks, siliciclastic rocks of all grain sizes;
- 3.2 - unconsolidated sediments (erodibility index details provided in Table 1).

A global map representing the erodibility index is shown in Fig. 2.

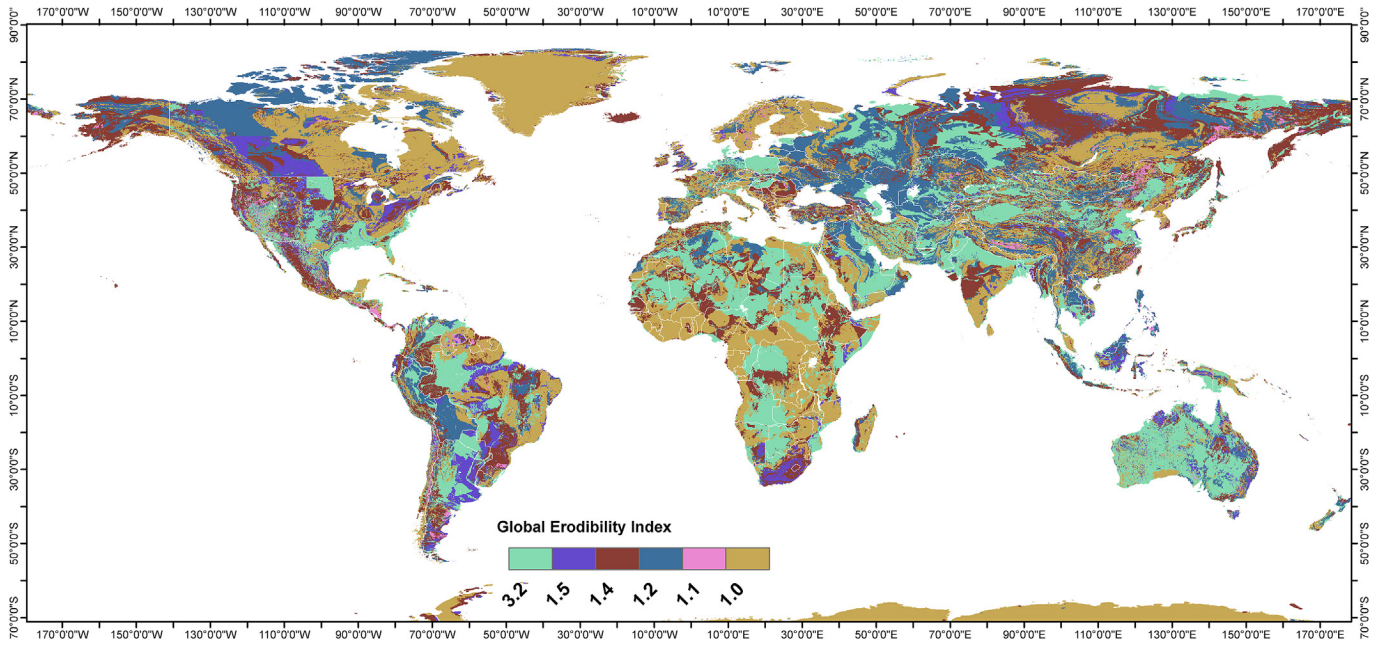

Fig. 2. A Map of the global erodibility index. The spatial distribution is based on the GLiM v1.0 lithological map (Hartmann & Moosdorf, 2012).

The lithological classes show a consistent erosion behavior throughout the different areas, represented by small standard deviations of the erodibility index (Table 1), despite large differences in tectonic and climatic regime. Some lithological classes, particularly basic plutonic rocks and coarse as well as fine-grained siliciclastic sediments, show larger variability of erodibility for different landscapes. For the erodibility index, the three subclasses of siliciclastic sediments (general, fine grained, coarse grained) shown in Table 1 were combined, because their distinction in the original lithological map is diffuse (Hartmann & Moosdorf, 2012; Moosdorf, Hartmann, & Dürr, 2010) and their erodibility similar. The highest range is noted for unconsolidated sediments, which at the same time also have the highest erodibility index. This may be a consequence of various factors influencing erodibility on local scale, such as vegetation cover or different consolidation state of largely unconsolidated sediments, which is not represented in this large scale study.

The slopes are substantially different between the analyzed landscapes. On average they are highest in the Himalayas, followed by Taiwan, Alps, Sierra Nevada, and the Mediterranean landscape (Table 1). The slopes were consistently higher for regions with higher rock uplift within a landscape (Table 1). This corroborates regional slopes correlate with rock uplift rate, which is consistent with studies from New Zealand and Nanga Parbat (Brocklehurst & Whipple, 2007) and the Olympic Mountains (Montgomery & Brandon, 2002). The sole exception is the Mediterranean high uplift area, where slopes are lower as compared to the low and medium uplift rate areas. However, in this area, only sedimentary lithological classes occur, which are less resistant to erosion and likely to show smaller average slopes.

Taiwan forms a special case in the analysis, as it is characterized by extremely high rock uplift rates and is often considered an archetype of a steady-state orogen (e.g. Byrne et al., 2011). Topographic analysis and modeling of the rock uplift pattern shows on orogen-scale there is little correlation between lithology and location of knick-zones in channels, indicating erosional efficiency is not primarily governed by rock type (Fox, Herman, Willett, & May, 2014). However, Fox et al. (2014) note that local deviations from predicted uplift rates exist and may be explained by rock type. Furthermore, a correlation between lithology and mean local slope has already been observed for the Taiwan Central Ranges (Stolar, Willett, & Montgomery, 2007).

3.2. Application example – global sediment flux modeling

The global erodibility index dataset was used as an input layer to the WBMsed model to demonstrate its applicability. The model sediment flux predictions using the GEroID were compared to the model predictions using the Syvitski and Milliman (2007) (S&M07) basin-lumped categorical values. Fig. 3 shows the percent difference in average suspended sediment flux predictions between the two simulations. Differences between the two simulations are considerable in many locations worldwide. This is expected considering the lack of adjustment in the index values and the model's L parameter. More interesting is the high spatial heterogeneity in many locations. This can be attributed to the higher spatial resolution of the GLiM input. In some areas, the two simulations differ over large extents (e.g. Scandinavia, northeast North America, and equatorial Africa). This may point to systematic differences between new global erodibility index and the original erodibility index for individual lithological classes (e.g. classified as high erodibility in one and low in the other) and/or differences in the underlying lithology maps. Boundary effects at country borders of the erodibility index can be observed where different source geological maps meet in the lithological map GLiM that have different geological units assigned at their boundaries. Adjacent geological maps are not harmonized regarding their unit boundaries even between different countries, or even between US states (Hartmann & Moosdorf, 2012; Moosdorf et al., 2010).

Fig. 4 shows the same percent difference calculation, masking all but large river reaches (contributing area over 20,000 km^2 and average discharge of over 30 m^3/s). This allows us to visualize the effect of using GEroID on sediment modeling for large river systems and demonstrate its effect on intra-basin dynamics. The difference between the two simulations is most pronounced in headwater areas (e.g. upper Amazon Basin), demonstrating a considerable increase in the model spatial explicitness. The main stems of large rivers are, in many cases, relatively unaffected (e.g. Amazon, Mississippi) by the erodibility input. This is due to increasing spatial averaging downstream, which lump the intra-basin variability in the GLiM lithology and consequently also in the GEroID (remember, S&M07 has one value for an entire basin). This observation is confirmed by comparing average sediment flux predictions by the two simulations at 202 river outlets worldwide. The strong correlation between the two simulations at river outlets (Fig. 5) shows

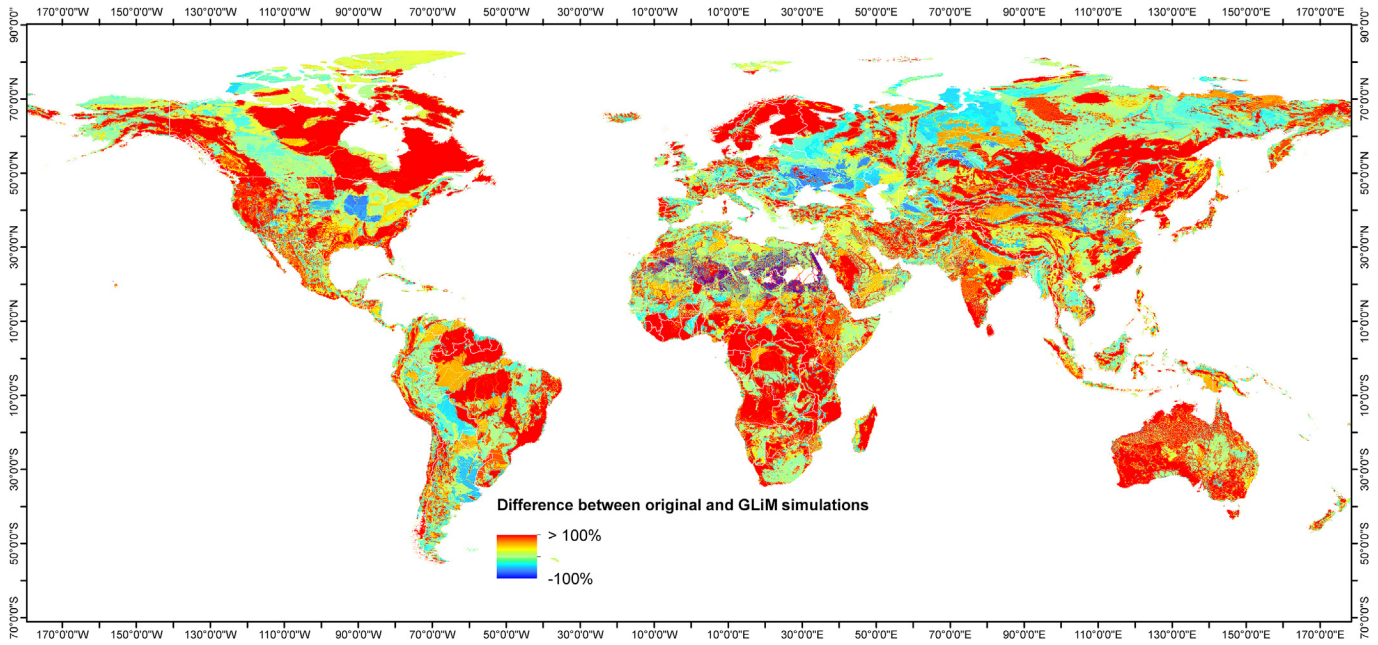

Fig. 3. Percent difference in suspended sediment flux predictions between the original and the GLiM simulations (calculated as 100 * ((S&M07 – GLiM)/S&M07)). Positive values indicate that the simulation using the original dataset predicted greater sediment flux.

that GEroID is consistent with S&M07 global variability but allow for a considerable greater degree of spatial explicitness.

3.3. Uncertainty analysis of the erodibility index

The presented erodibility index is a simple tool to estimate the relative erodibility of rock types for given environmental conditions at large scales, which obviously includes uncertainties. Uncertainties we are unable to quantify are those regarding geological boundaries in the lithological map, or effects of uplift class definition. We also note that as we used the present day lithological map, results of this study should only be applied to timescales where no change of exposed rock type at the scale of the mapped areas is expected. For paleo-erodibility maps representative for longer timescales, i.e. millions of years, paleo-lithological maps would be required. In addition, slope is affected by other factors beyond rock erosivity and tectonic uplift which are not represented in this study. Climate (Carretier et al., 2013; Schmidt & Dikau, 2004) and vegetation (Prandini, Guidiini, Bottura, Pançano, & Santos, 1977; Schwarz, Preti, Giadrossich, Lehmann, & Or, 2010) are major additional controls. However, the regions are small enough that no significant climatic or land-cover bias is expected between the lithological classes. The usage of primarily mountainous terrain for calibration may inhibit the use of the erodibility index in lowland areas. However, these are mostly dominated by unconsolidated lithologies,

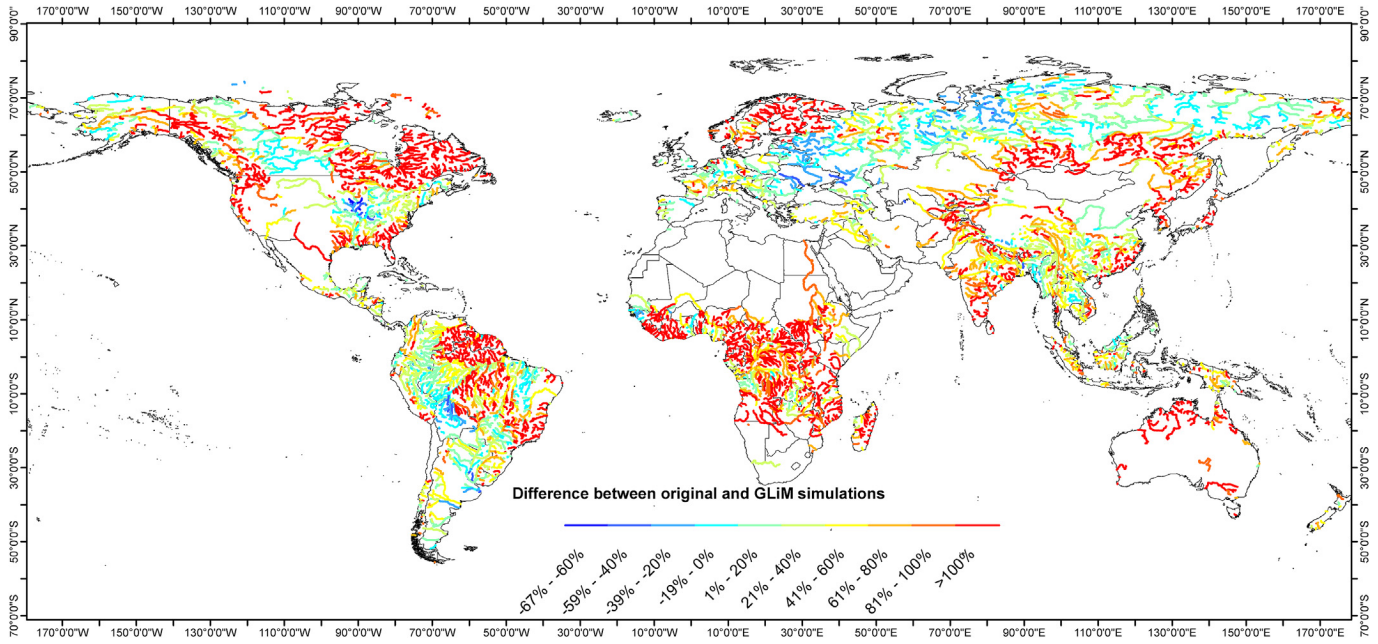

Fig. 4. Percent difference in suspended sediment flux predictions between the original and the new erodibility index simulations in large rivers only showing rivers with contributing area > 10,000 km^2 and average water discharge > 30 m^3/s). Positive values indicate that the simulation using the original dataset predicted greater sediment flux.

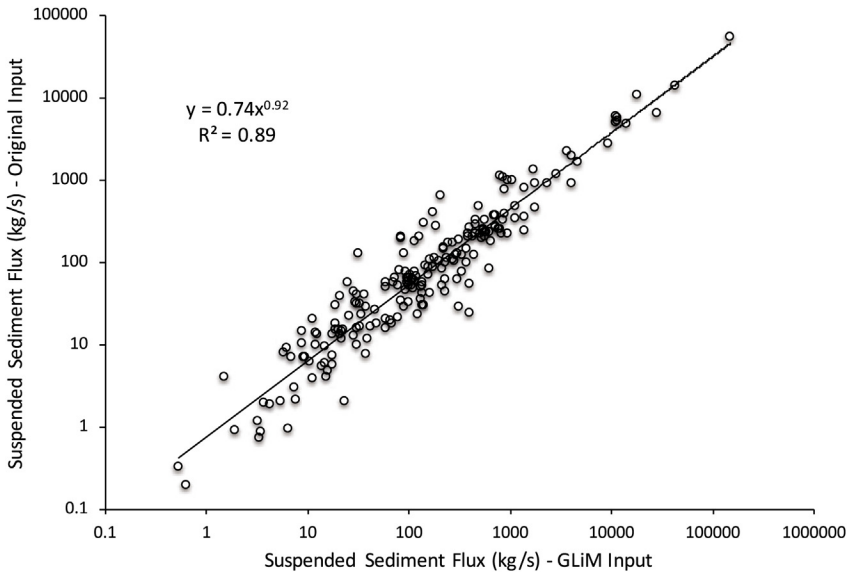

Fig. 5. Sediment flux predictions using the original lithology input vs. Using GLiM in 202 global river coastal outlets.

and natural sediment mobilization from lowlands is far smaller than from mountainous areas (Koppes & Montgomery, 2009).

One uncertainty that can be quantified is the uncertainty of the DEM, which affects slopes and other geomorphological parameters (e.g. Poggio & Gimona, 2014; Temme et al., 2009). For all landscapes, a Monte Carlo Analysis assessing the effect of DEM uncertainty (of + - 10 m) on slopes and thus on the erodibility index was performed. Averaging of slopes over very large areas performed in this study strongly reduces its sensitivity to DEM errors. A table showing all used slopes and their standard deviations is added as electronic supplement. It demonstrates that the standard deviations of average slopes for individual lithological classes and regions average 0.01° (maximum: 0.4° for pb in the Taiwan medium uplift region, see electronic supplement), which results from averaging slopes of an average area of 4000 km^2 per lithology and region. Thus, contrary to spatially explicit methods, where the DEM error of each individual cell has to be regarded, in this case the effect of the DEM error is negligible and only a minor part of the total uncertainty of the erodibility index. The Monte Carlo Simulation based on the slope variability shows that the impact of DEM uncertainty on the erodibility index is negligible (on average the resulting standard deviations of the erodibility index are 0.0014). Thus, the dominating uncertainty in the erodibility index lies in the difference between landscapes, due to different environmental parameters.

A one-way ANOVA analysis confirmed that the erodibility index for individual lithological classes between the analyzed regions is statistically equal ($p = 0.68$) while it is statistically different between the lithological classes ($p < 0.001$). Despite this stable appearance at global scale, the presented erodibility index should not be used at the local scale, because it may not sufficiently represent the local attributes of the considered lithologies.

3.4. Evaluation against local observations

The presented new erodibility index quantifies large-scale erodibility potential for different lithological units from a recently published global lithology map (GLiM v1.0 (Hartmann & Moosdorf, 2012)). The index is based on slope values from a digital elevation model with a horizontal resolution of 30 m. Although the absolute slope values are highly scale sensitive (e.g. Zhang, Drake, Wainwright, & Mulligan, 1999), the normalization of the erodibility index against acid plutonics (Eq. (1)) should reduce this effect. Nevertheless, if there is a scale effect, it should lead to a smaller erodibility index compared to local scale studies with higher spatial resolution, because mapped slopes tend to be smaller with decreasing resolution (as local variations of topography are averaged out), leading to a smaller slope difference and erodibility index. The same is true for the lithological base data, which does not resolve the finest occurrences of different rock units but uses data mostly of a scale of about 1:1 million. Thus, the erodibility index for a lithological unit is not strictly comparable to measures of erodibility of similarly named rock types at local scale, because the lithological units actually can encompass a whole suite of different rocks. Although this is the highest resolved global lithology map available, compared to finer resolved local maps, the erodibility index should thus be moderated, as e.g. shown for silicate flux and a comparison of different lithological datasets (Moosdorf et al., 2010). A similar error may have been introduced by spatial averaging of rock uplift rates. These are commonly point measurements, and interpolating between these points may mask true local variations in uplift. On the other hand, very local measurements may not be representative for the global scale erodibility index, as they may record transient high uplift rates at a single fault due to single earthquake events. Spatial averaging reduces this possible bias of the recorded rock uplift signal. Given the scale effect, it is expected that the erodibility index difference of 1.5 between sedimentary rocks and crystalline rocks is below the difference between their rock mass strength index identified in a detail study of an alpine region (Korup & Schlunegger, 2009). At local scale, rock attributes like mineralogy or joints and fractures influence erodibility (e.g. Goode & Wohl, 2010; Selby, 1980). Substrate lithology can influence the dominant erosion process (Whipple, Hancock, & Anderson, 2000), which in turn determines the rock attributes controlling erodibility (e.g. Lamb, Finnegan, Scheingross, & Sklar, 2015). However, at global scale no data are available to represent the input values needed for local scale estimates, such as the rock mass strength index.

In some landscapes, vegetation is the primary source of variability of erosion; for instance in the San Gabriel Mountains, CA wildfires and consequent presence or absence of vegetation control recurrence intervals of landslides (Lamb, Scheingross, Amidon, Swanson, & Limaye, 2011). Likewise, it has been shown that the bulk erosional flux in some landscapes results from large earthquakes with a recurrence interval of several hundreds or thousands of years (Parker et al., 2011). Correlation between dry climate and slow erosion is well known (Bierman & Caffee, 2001), and climate may influence erosion on various timescales (Ganti et al., 2016). Climate may also vary within a landscape, albeit to much smaller degree as compared to different landscapes in different

climatic regions. Regarding this variability, the consistent patterns of erodibility across multiple landscapes seem surprising. Similarly, Harel et al. (2016) note lack of correlation between precipitation and erodibility on a global scale. Even though correlations between climate and erodibility may exist, they possibly counterbalance each other, which may explain the lack of correlation. This underscores the importance of lithology as one major factor controlling sediment production.

A regional scale study from Brittany, France, also determined erodibility based on slope (Lague et al., 2000). That study differentiates three lithologies: weathered granite, schist, as well as "gneiss and sandstone", whose erodibility (normalized to the weathered granite) is: 1, 0.53, and 0.31, respectively. The results of (Lague et al., 2000) in their regional study differ from the here presented erodibility index, which highlights the local variability of rock erodibility, e.g. due to regionally different state of weathering. At the large scale, individual bedrock lithologies are integrated from individual rocks into rock units, and dominant erosion processes are combined at the resolution of the global datasets, which is up to 1 km^2. Thus, erodibility at this scale needs to be an empirical integration of the different aspects known from local scale, using available datasets. Here we propose that an erodibility index calibrated on hillslope can be used to differentiate between the erodibility of different lithological units at global scale.

4. Conclusions

We propose the global erodibility index to describe large scale erodibility potential of different lithological classes, based on slope. The index was calibrated in different landscapes around the globe, including tectonically active and inactive areas, as well as different climatic regions. Within these landscapes regions of homogenous rock uplift were defined based on published maps of orogen-scale rock uplift. It shows that the erodibility of rocks relative to acid plutonics (granite) varies by a factor of 3.2, with unconsolidated sediments showing the highest erodibility and acid volcanics exhibiting the lowest.

The new erodibility index can be compared to locally focused indices of rock stability as the Rock Mass Strength Index (Selby, 1980) or the Geological Strength Index (Marinos, Marinos, & Hoek, 2005), which are estimated based on field values. However, primarily it should provide a basis to distinguish the effect of different rock types for large scale erosion and sediment dynamic modeling. It can be used in a variety of studies analyzing large scale geomorphology-related processes and dynamics. This was demonstrated in this study by incorporating the new global erodibility index dataset (GEroID) in a global sediment flux model showing a considerable increase in the spatial representation of the model's lithology parameter without considerable alteration to its global predictions.

Acknowledgements

NM was supported through the German Federal Ministry of Education and Research (grant #01LN1307A); SC was partly supported by a grant from the National Science Foundation (#1561082).

This paper is based on ASTER GDEM elevation data products, downloadable at several sites, e.g. http://www.jspacesystems.or.jp/ersdac/GDEM/E/index.html. The new global erodibility index dataset (GEroID) gridded to the resolution of the WBMSed model is linked to this dataset. Using the original source lithology dataset and the erodibility indices for each lithology class, other grid resolutions can be generated.

Three anonymous reviewers are acknowledged for constructive comments, which helped improving the manuscript. M. Patterson and Nancy Hoalst-Pullen are acknowledged for editorial handling of the manuscript.

Appendix A. Supplementary data

Supplementary data to this article can be found online at https://doi.org/10.1016/j.apgeog.2018.10.010.

References

Acosta, V. T., Schildgen, T. F., Clarke, B. A., Scherler, D., Bookhagen, B., Wittmann, H., et al. (2015). Effect of vegetation cover on millennial-scale landscape denudation rates in East Africa. *Lithosphere-Us, 7*, 408–420.

Avouac, J. P. (2008). Dynamic processes in extensional and compressional settings - mountain building: From earthquakes to geological deformation. *Treatise on Geophysics, 6*, 377–439.

Bierman, P. R., & Caffee, M. (2001). Slow rates of rock surface erosion and sediment production across the Namib Desert and escarpment, southern Africa. *American Journal of Science, 301*, 326–358.

von Blanckenburg, F. (2005). The control mechanisms of erosion and weathering at basin scale from cosmogenic nuclides in river sediment. *Earth and Planetary Science Letters, 237*, 462–479.

Braun, J. (2010). The many surface expressions of mantle dynamics. *Nature Geoscience, 3*, 825–833.

Braun, J., Simon-Labric, T., Murray, K. E., & Reiners, P. W. (2014). Topographic relief driven by variations in surface rock density. *Nature Geoscience, 7*, 534–540.

Brocklehurst, S. H., & Whipple, K. X. (2007). Response of glacial landscapes to spatial variations in rock uplift rate. *Journal of Geophysical Research-Earth Surface, 112*.

Byrne, T. B., Chan, Y. C., Rau, R.-J., Lu, C. Y., Lee, Y.-H., & Wang, Y.-J. (2011). the Arc-continent collision in Taiwan. In D. Brown, & P. Ryan (Eds.). *Arc-continent collision* (pp. 213–245). Berlin: Springer.

Carretier, S., Regard, V., Vassallo, R., Aguilar, G., Martinod, J., Riquelme, R., et al. (2013). Slope and climate variability control of erosion in the Andes of central Chile. *Geology, 41*, 195–198.

Cerdan, O., Govers, G., Le Bissonnais, Y., Van Oost, K., Poesen, J., Saby, N., et al. (2010). Rates and spatial variations of soil erosion in Europe: A study based on erosion plot data. *Geomorphology, 122*, 167–177.

Champagnac, J. D., Schlunegger, F., Norton, K., von Blanckenburg, F., Abbuhl, L. M., & Schwab, M. (2009). Erosion-driven uplift of the modern central alps. *Tectonophysics, 474*, 236–249.

Ching, K. E., Hsieh, M. L., Johnson, K. M., Chen, K. H., Rau, R. J., & Yang, M. (2011). Modern vertical deformation rates and mountain building in Taiwan from precise leveling and continuous GPS observations, 2000-2008. *Journal of Geophysical Research-Solid Earth, 116*.

Cohen, S., Kettner, A. J., & Syvitski, J. P. M. (2014). Global suspended sediment and water discharge dynamics between 1960 and 2010: Continental trends and intra-basin sensitivity. *Global and Planetary Change, 115*, 44–58.

Cohen, S., Willgoose, G., & Hancock, G. (2013). Soil-landscape response to mid and late Quaternary climate fluctuations based on numerical simulations. *Quaternary Research, 79*, 452–457.

Cook, K. L., Turowski, J. M., & Hovius, N. (2013). A demonstration of the importance of bedload transport for fluvial bedrock erosion and knickpoint propagation. *Earth Surface Processes and Landforms, 38*, 683–695.

Dadson, S. J., Hovius, N., Chen, H., Dade, W. B., Hsieh, M.-L., Willett, S. D., et al. (2003). Links between erosion, runoff variability and seismicity in the Taiwan orogen. *Nature, 426*, 648–651.

Deal, E., Favre, A.-C., & Braun, J. (2017). Rainfall variability in the Himalayan orogen and its relevance to erosion processes. *Water Resources Research, 53*. https://doi.org/10.1002/2016WR020030.

DiBiase, R. A., Whipple, K., Heimsath, A. M., & Ouimet, W. B. (2010). Landscape form and millennial erosion rates in the San Gabriel Mountains, CA. *Earth and Planetary Science Letters, 289*, 134–144.

Douglas, I. A. N. (1967). Man, vegetation and the sediment yields of rivers. *Nature, 215*, 925–928.

Dürr, H. H., Meybeck, M., & Dürr, S. H. (2005). Lithologic composition of the Earth's continental surfaces derived from a new digital map emphasizing riverine material transfer. *Global Biogeochemical Cycles, 19*, GB4S10.

England, P., & Molnar, P. (1990). Surface uplift, uplift of rocks, and exhumation of rocks. *Geology, 18*, 1173–1177.

Fjeldskaar, W., Lindholm, C., Dehls, J. F., & Fjeldskaar, I. (2000). Postglacial uplift, neotectonics and seismicity in Fennoscandia. *Quaternary Science Reviews, 19*, 1413–1422.

Flanagan, D. C., & Nearing, M. A. (1995). *USDA Water Erosion Prediction Project hillslope and watershed model documentation*NSERL Report No. 10. West-Lafayette, Ind: USDA-ARS National Soil Erosion Research Laboratory.

Fox, M., Herman, F., Willett, S. D., & May, D. A. (2014). A linear inversion method to infer exhumation rates in space and time from thermochronometric data. *Earth Surface Dynamics, 2*, 47–65.

Gaillardet, J., Dupre, B., Allegre, C. J., & Negrel, P. (1997). Chemical and physical denudation in the Amazon River basin. *Chemical Geology, 142*, 141–173.

Ganti, V., Von Hagke, C., Scherler, D., Lamb, M. P., Fischer, W. W., & Avouac, J.-P. (2016). Time scale bias in erosion rates of glaciated landscapes. *Science Advances, 2*(10).

Geological and Geographical Survey of the Territories (U.S.). (1876). *Report on the geology of the eastern portion of the Uinta Mountains and a region of country adjacent thereto. With atlas*Washington: Gov't print. off.

Goode, J. R., & Wohl, E. (2010). Substrate controls on the longitudinal profile of bedrock

channels: Implications for reach-scale roughness. *Journal of Geophysical Research-Earth Surface, 115*.
Hager, B. H., Clayton, R. W., Richards, M. A., Comer, R. P., & Dziewonski, A. M. (1984). Lower mantle heterogeneity, dynamic topography and the geoid. *Nature, 313*, 541–545.
von Hagke, C., Oncken, O., Ortner, H., Cederbom, C. E., & Aichholzer, S. (2014). Late Miocene to present deformation and erosion of the Central Alps — evidence for steady state mountain building from thermokinematic data. *Tectonophysics, 632*, 250–260.
Hammond, W. C., Blewitt, G., Li, Z. H., Plag, H. P., & Kreemer, C. (2012). Contemporary uplift of the Sierra Nevada, western United States, from GPS and InSAR measurements. *Geology, 40*, 667–670.
Harel, M. A., Mudd, S. M., & Attal, M. (2016). Global analysis of the stream power law parameters based on worldwide 10Be denudation rates. *Geomorphology, 268*, 184–196.
Hartmann, J., & Moosdorf, N. (2012). The new global lithological map database GLiM: A representation of rock properties at the Earth surface. *Geochemistry, Geophysics, Geosystems, 13*, Q12004.
Hartshorn, K., Hovius, N., Dade, W. B., & Slingerland, R. L. (2002). Climate-driven bedrock incision in an active mountain belt. *Science, 297*, 2036–2038.
Herman, F., Seward, D., Valla, P. G., Carter, A., Kohn, B., Willett, S. D., et al. (2013). Worldwide acceleration of mountain erosion under a cooling climate. *Nature, 504*, 423–426.
Koppes, M. N., & Montgomery, D. R. (2009). The relative efficacy of fluvial and glacial erosion over modern to orogenic timescales. *Nature Geoscience, 2*, 644.
Korup, O., & Schlunegger, F. (2009). Rock-type control on erosion-induced uplift, eastern Swiss Alps. *Earth and Planetary Science Letters, 278*, 278–285.
Kühni, A., & Pfiffner, O. A. (2001). The relief of the Swiss alps and adjacent areas and its relation to lithology and structure: Topographic analysis from a 250-m DEM. *Geomorphology, 41*, 285–307.
Lague, D., Davy, P., & Crave, A. (2000). Estimating uplift rate and erodibility from the area-slope relationship: Examples from Brittany (France) and numerical modelling. *Physics and Chemistry Earth Part A, 25*, 543–548.
Lamb, M. P., Finnegan, N. J., Scheingross, J. S., & Sklar, L. S. (2015). New insights into the mechanics of fluvial bedrock erosion through flume experiments and theory. *Geomorphology, 244*, 33–55.
Lamb, M. P., Scheingross, J. S., Amidon, W. H., Swanson, E., & Limaye, A. (2011). A model for fire-induced sediment yield by dry ravel in steep landscapes. *Journal of Geophysical Research: Earth Surface, 116*, F03006.
Marinos, V., Marinos, P., & Hoek, E. (2005). The geological strength index: Applications and limitations. *Bulletin of Engineering Geology and the Environment, 64*, 55–65.
Meybeck, M. (1987). Global chemical weathering of surficial rocks estimated from river dissolved loads. *American Journal of Science, 287*, 401–428.
Milliman, J. D., Qin, Y. S., Ren, M. E., & Saito, Y. (1987). Mans influence on the erosion and transport of sediment by Asian rivers - the Yellow-river (Huanghe) example. *The Journal of Geology, 95*, 751–762.
Milliman, J. D., & Syvitski, J. P. M. (1992). Geomorphic tectonic control of sediment discharge to the ocean - the importance of small mountainous rivers. *The Journal of Geology, 100*, 525–544.
Molnar, P., & England, P. (1990). Late cenozoic uplift of mountain ranges and global climate change: Chicken or egg? *Nature, 346*, 29–34.
Montgomery, D. R., & Brandon, M. T. (2002). Topographic controls on erosion rates in tectonically active mountain ranges. *Earth and Planetary Science Letters, 201*, 481–489.
Moosdorf, N., Hartmann, J., & Dürr, H. H. (2010). Lithological composition of the North American continent and implications of lithological map resolution for dissolved silica flux modeling. *Geochemistry, Geophysics, Geosystems, 11*, Q11003.
Mukul, M., Srivastava, V., Jade, S., & Mukul, M. (2017). Uncertainties in the shuttle radar topography mission (SRTM) Heights: Insights from the indian Himalaya and Peninsula. *Scientific Reports, 7*.
Parker, R. N., Densmore, A. L., Rosser, N. J., de Michele, M., Li, Y., Huang, R., et al. (2011). Mass wasting triggered by the 2008 Wenchuan earthquake is greater than orogenic growth. *Nature Geoscience, 4*, 449–452.
Poggio, L., & Gimona, A. (2014). National scale 3D modelling of soil organic carbon stocks with uncertainty propagation — an example from Scotland. *Geoderma, 232–234*, 284–299.
Portenga, E. W., & Bierman, P. R. (2011). Understanding Earth's eroding surface with 10Be. *Geological Society of America Today, 21*, 4–10.
Prandini, L., Guidiini, G., Bottura, J. A., Pançano, W. L., & Santos, A. R. (1977). Behavior of the vegetation in slope stability: A critical review. *Bulletin of the International Association of Engineering Geology, 16*, 51–55 Bulletin de l'Association Internationale de Géologie de l'Ingénieur.
Raymo, M. E., Ruddiman, W. F., & Froelich, P. N. (1988). Influence of late cenozoic mountain building on ocean geochemical cycles. *Geology, 16*, 649–653.
Reiners, P. W., & Brandon, M. T. (2006). Using thermochronology to understand orogenic erosion. *Annual Review of Earth and Planetary Sciences, 34*, 419–466.
Renard, K. G., Foster, G. R., Weesies, G. A., & Porter, J. P. (1991). Rusle - revised universal soil loss equation. *Journal of Soil & Water Conservation, 46*, 30–33.
Sadler, P. M. (1981). Sediment accumulation rates and the completeness of stratigraphic sections. *The Journal of Geology*, 569–584.
Saunders, I., & Young, A. (1983). Rates of surface processes on slopes, slope retreat and denudation. *Earth Surface Processes and Landforms, 8*, 473–501.
Schaller, M., von Blanckenburg, F., Hovius, N., & Kubik, P. W. (2001). Large-scale erosion rates from in situ-produced cosmogenic nuclides in European river sediments. *Earth and Planetary Science Letters, 188*, 441–458.
Schlatter, A., Schneider, D., Geiger, A., & Kahle, H. G. (2005). Recent vertical movements from precise levelling in the vicinity of the city of Basel, Switzerland. *International Journal of Earth Sciences, 94*, 507–514.
Schmidt, J., & Dikau, R. (2004). Modeling historical climate variability and slope stability. *Geomorphology, 60*, 433–447.
Schumer, R., & Jerolmack, D. J. (2009). Real and apparent changes in sediment deposition rates through time. *Journal of Geophysical Research: Earth Surface, 114*, F00A06.
Schwarz, M., Preti, F., Giadrossich, F., Lehmann, P., & Or, D. (2010). Quantifying the role of vegetation in slope stability: A case study in Tuscany (Italy). *Ecological Engineering, 36*, 285–291.
Selby, M. J. (1980). A rock mass strength classification for geomorphic purposes with tests from Antarctica and New Zealand. *Zeitschrift für Geomorphologie, 24*, 31–51.
Serpelloni, E., Faccenna, C., Spada, G., Dong, D., & Williams, S. D. P. (2013). Vertical GPS ground motion rates in the Euro-Mediterranean region: New evidence of velocity gradients at different spatial scales along the Nubia-Eurasia plate boundary. *Journal of Geophysical Research: Solid Earth, 118*, 6003–6024.
Sklar, L. S., & Dietrich, W. E. (2001). Sediment and rock strength controls on river incision into bedrock. *Geology, 29*, 1087–1090.
Stevens, V. L., & Avouac, J. P. (2015). Interseismic coupling on the main Himalayan thrust. *Geophysical Research Letters, 42*, 5828–5837.
Stolar, D. B., Willett, S. D., & Montgomery, D. R. (2007). Characterization of topographic steady state in Taiwan. *Earth and Planetary Science Letters, 261*, 421–431.
Syvitski, J. P. M., & Milliman, J. D. (2007). Geology, geography, and humans battle for dominance over the delivery of fluvial sediment to the coastal ocean. *The Journal of Geology, 115*, 1–19.
Temme, A. J. A. M., Heuvelink, G. B. M., Schoorl, J. M., & Claessens, L. (2009). Chapter 5 geostatistical simulation and error propagation in geomorphometry. In T. Hengl, & H. I. Reuter (Eds.). *Developments in soil science* (pp. 121–140). Elsevier.
Tucker, G. E., & Bras, R. L. (2000). A stochastic approach to modeling the role of rainfall variability in drainage basin evolution. *Water Resources Research, 36*, 1953–1964.
Tucker, G., Lancaster, S., Gasparini, N., & Bras, R. (2001). *The channel-hillslope integrated landscape development model (CHILD), Landscape erosion and evolution modeling.* Springer349–388.
Turowski, J. M., Hovius, N., Meng-Long, H., Lague, D., & Men-Chiang, C. (2008). Distribution of erosion across bedrock channels. *Earth Surface Processes and Landforms, 33*, 353–363.
de Vente, J., & Poesen, J. (2005). Predicting soil erosion and sediment yield at the basin scale: Scale issues and semi-quantitative models. *Earth-Science Reviews, 71*, 95–125.
de Vente, J., Poesen, J., Verstraeten, G., Govers, G., Vanmaercke, M., Van Rompaey, A., et al. (2013). Predicting soil erosion and sediment yield at regional scales: Where do we stand? *Earth-Science Reviews, 127*, 16–29.
West, A. J., Galy, A., & Bickle, M. (2005). Tectonic and climatic controls on silicate weathering. *Earth and Planetary Science Letters, 235*, 211–228.
Whipple, K. (2009). The influence of climate on the tectonic evolution of mountain belts. *Nature Geoscience, 2*, 97–104.
Whipple, K., Hancock, G. S., & Anderson, R. S. (2000). River incision into bedrock: Mechanics and relative efficacy of plucking, abrasion, and cavitation. *The Geological Society of America Bulletin, 112*, 490–503.
Whipple, K., & Meade, B. J. (2006). Orogen response to changes in climatic and tectonic forcing. *Earth and Planetary Science Letters, 243*, 218–228.
Whipple, K., & Tucker, G. E. (2002). Implications of sediment-flux-dependent river incision models for landscape evolution. *Journal of Geophysical Research: Solid Earth, 107*.
Willett, S. D., & Brandon, M. T. (2002). On steady states in mountain belts. *Geology, 30*, 175–178.
Wittmann, H., von Blanckenburg, F., Kruesmann, T., Norton, K. P., & Kubik, P. W. (2007). Relation between rock uplift and denudation from cosmogenic nuclides in river sediment in the Central Alps of Switzerland. *Journal of Geophysical Research, 112*, F04010.
Wright, V. P., & Marriott, S. B. (1993). The sequence stratigraphy of fluvial depositional systems: The role of floodplain sediment storage. *Sedimentary Geology, 86*, 203–210.
Yanites, B. J., Tucker, G. E., Hsu, H. L., Chen, C.c., Chen, Y. G., & Mueller, K. J. (2011). The influence of sediment cover variability on long-term river incision rates: An example from the Peikang River, central Taiwan. *Journal of Geophysical Research: Earth Surface, 116*.
Zhang, X. Y., Drake, N. A., Wainwright, J., & Mulligan, M. (1999). Comparison of slope estimates from low resolution DEMs: Scaling issues and a fractal method for their solution. *Earth Surface Processes and Landforms, 24*, 763–779.